Geophys. J. Int. (2008) **175,** 477–485 doi: 10.1111/j.1365-246X.2008.03894.x

Efficient three-dimensional inversion of magnetotelluric data using approximate sensitivities

Nuree Han,[1] Myung Jin Nam,[2]* Hee Joon Kim,[3] Tae Jong Lee,[4]† Yoonho Song[4] and Jung Hee Suh[5]

[1]*Department of Civil, Urban and Geosystem Engineering, Seoul National University, Korea. E-mail: world3@snu.ac.kr*
[2]*Department of Petroleum and Geosystems Engineering, The University of Texas at Austin, USA*
[3]*Department of Environmental Exploration Engineering, Pukyong National University, Korea*
[4]*Groundwater and Geothermal Resources Division, Korea Institute of Geoscience and Mineral Resources, Korea. E-mail: megi@kigam.re.kr*
[5]*Deceased, Formerly Department of Civil, Urban and Geosystem Engineering, Seoul National University, Korea*

Accepted 2008 June 24. Received 2008 June 24; in original form 2008 January 31

SUMMARY

A method for accurately approximating sensitivities is introduced for the efficient 3-D inversion of static-shifted magnetotelluric (MT) data. Approximate sensitivities are derived by replacing adjoint secondary electric fields with those computed in the previous iteration. These sensitivities can reduce the computation time, without significant loss of accuracy when constructing a full sensitivity matrix for 3-D inversion, based on the Gauss–Newton method. Additional reduction of computational cost can be attained by modifying the inversion scheme to run on a parallel computing platform. The effectiveness of approximate sensitivities is tested by inverting both synthetic and field data obtained in Pohang, Korea, and Bajawa, Indonesia. The accuracy of approximate sensitivities is validated by sensitivity analysis of synthetic data. To make the inversion of static-shifted MT data more stable, a weighting coefficient for static-shift parameters is added to the objective function and is updated at each iteration. Approximate sensitivities are calculated much faster than exact sensitivities, and are accurate enough to drive an iterative inversion algorithm.

Key words: Inverse theory; Numerical approximations and analysis; Magnetotelluric.

1 INTRODUCTION

A reliable and efficient scheme for 3-D interpretation of magnetotelluric (MT) data is increasingly important because of growing applications of 3-D surveys investigating the subsurface structure (Takasugi *et al*. 1992; Uchida *et al*. 2002; Lee *et al*. 2007). Traditional MT inversion methods based on the Gauss–Newton (GN) approach are too expensive to be used as a rigorous 3-D interpretation tool because constructing a sensitivity matrix requires too much computation time. As a result, reliable 3-D interpretation of MT data is not widely used, and MT data are commonly interpreted using 2-D inversion for various profiles (Garcia *et al*. 1999; Tournerie & Chouteau 2005).

Many researchers have produced practical 3-D MT inversion schemes over the last decade. Zhdanov *et al*. (2000) developed a rapid 3-D inversion algorithm, based on the quasi-linear approximation of Green's function. Smith & Booker (1991) developed a scheme called rapid relaxation inversion, using approximate (1-D) sensitivities. Farquharson & Oldenburg (1999) also used approximate sensitivities that were computed from adjoint fields for a homogeneous or layered half-space. By using a conjugate gradient (CG) method, the explicit computation and storage of a full sensitivity matrix can be avoided (Mackie & Madden 1993; Newman & Alumbaugh 2000). Rodi & Mackie (2001) demonstrated that CG-based algorithms can be more practical in terms of computation time. Sasaki (2004) and Siripunvaraporn *et al*. (2005) have developed alternative approaches to the 3-D inverse problem and have described practical 3-D inversions based on the GN-type approach in model- and data-space, respectively.

In a conventional GN-type inversion, the majority of computation time is spent in constructing a full sensitivity matrix. Although the efficient adjoint-equation method is used (McGillivray *et al*. 1994), a larger number of forward calculations are required, especially for 3-D. To make 3-D inversion practical, a reduction of computation time is necessary. This paper shows that approximate sensitivities can be used to decrease the total number of forward calculations required in a 3-D inversion. The approximate sensitivities are computed by replacing the secondary electric fields with those computed in the previous iteration. The computational cost can be further reduced when a parallel computing scheme is implemented.

This paper first describes the inversion and forward modelling algorithms. The following explains the methods used to compute the approximate sensitivities and to implement the parallel computation. It is shown that approximate sensitivities compare well with

*Formerly at: Korea Institute of Geoscience and Mineral Resources, Korea.
†Corresponding author.

exact values, through sensitivity analysis using synthetic MT data. Finally, approximate sensitivities are tested on MT data measured in Pohang, Korea, and Bajawa, Indonesia, to confirm the effectiveness of reconstructing reasonable resistivity images.

2 INVERSION ALGORITHM

The MT inverse problem is non-linear with respect to subsurface electrical properties and is generally solved iteratively. The MT inverse problem with static shifts can be linearized as

$$\Delta\mathbf{d} = \mathbf{J}\Delta\mathbf{m} + \mathbf{G}\mathbf{s}, \tag{1}$$

where $\Delta\mathbf{d}$ is a vector of differences between observed and predicted data, $\Delta\mathbf{m}$ is a model correction vector, $\mathbf{J}$ is a sensitivity matrix, $\mathbf{s}$ is a vector of static-shift parameters and $\mathbf{G}$ is a matrix which relates $\mathbf{s}$ to observed data (deGroot-Hedlin 1991; Ogawa & Uchida 1996).

Because eq. (1) can be numerically unstable when solved for $\Delta\mathbf{m}$, it is necessary to apply constraints to obtain a solution. A widely used constraint is to minimize model roughness through the objective function Φ (Sasaki 2004)

$$\Phi = \|\mathbf{W}_d(\mathbf{J}\Delta\mathbf{m} + \mathbf{G}\mathbf{s} - \Delta\mathbf{d})\|^2 + \lambda^2[\|\mathbf{R}\mathbf{m}^{k+1}\|^2 + \alpha^2\|\mathbf{m}^{k+1} - \mathbf{m}_b\|^2] + \beta^2\|\mathbf{s}\|^2, \tag{2}$$

where $\mathbf{W}_d$ is a diagonal matrix whose elements are the reciprocal of measurement uncertainties, $\mathbf{R}$ is a second-order difference operator quantifying model roughness, $\mathbf{m}^{k+1}$ is the $(k+1)$th model, being determined simultaneously with $\mathbf{s}$, to minimize Φ. Here $\mathbf{m}_b$ can be either a base model or the model of the previous iteration, $\mathbf{m}^k$, and λ, α and β are trade-off parameters. Static shifts are assumed to have a Gaussian distribution (Ogawa & Uchida 1996).

In eq. (2), the term β controls the weighting of the static shifts and is fixed throughout the inversion process. In contrast, $\boldsymbol{\lambda}$ is selected to yield a model with minimum data misfit at each iteration. As we demonstrate below, it is necessary to change the weighting factor as the inversion proceeds to accurately recover static shifts since λ varies widely during inversion. Thus, eq. (2) is modified as (Lee *et al*. 2003)

$$\Phi = \|\mathbf{W}_d(\mathbf{J}\Delta\mathbf{m} + \mathbf{G}\mathbf{s} - \Delta\mathbf{d})\|^2 + \lambda^2[\|\mathbf{R}\mathbf{m}^{k+1}\|^2 + \alpha^2\|\mathbf{m}^{k+1} - \mathbf{m}_b\|^2 + \beta^2\|\mathbf{s}\|^2]. \tag{3}$$

Note as the weighting to static shifts, $\lambda\beta$ varies while β remains constant.

Minimizing Φ in eq. (3) is equivalent to solving an observation equation

$$\begin{bmatrix} \mathbf{W}_d\mathbf{J} & \mathbf{W}_d\mathbf{G} \\ \lambda\mathbf{R} & \mathbf{0} \\ \lambda\alpha\mathbf{I} & \mathbf{0} \\ \mathbf{0} & \lambda\beta\mathbf{I} \end{bmatrix} \begin{bmatrix} \mathbf{m}^{k+1} \\ \mathbf{s} \end{bmatrix} = \begin{bmatrix} \mathbf{W}_d(\mathbf{J}\mathbf{m}^k + \Delta\mathbf{d}) \\ \mathbf{0} \\ \lambda\alpha\mathbf{m}_b \\ \mathbf{0} \end{bmatrix}, \tag{4}$$

where $\mathbf{I}$ is the identity matrix. The modified Gram–Schmidt method is used to solve eq. (4). The iteration is continued until either a specific number of iteration is met or a root-mean-square (rms) misfit measure is reduced to acceptable level.

The rms data misfit is defined as

$$R = \sqrt{\frac{\Delta\mathbf{d}^{\mathrm{T}}\mathbf{W}_{\mathbf{d}}^{\mathrm{T}}\mathbf{W}_d\Delta\mathbf{d}}{N}}, \tag{5}$$

where N is the number of data. Components of $\mathbf{W}_d$ are defined as reciprocals of standard deviations of observed data errors. If data errors are not available, then eq. (5) is modified as

$$R = \sqrt{\frac{\sum_{i=1}^{N/2}\left\{\left[\ln\left(\rho_{ai}^{\mathrm{o}}/\rho_{ai}^{\mathrm{p}}\right)\right]^2 + w^2\left(\phi_i^{\mathrm{o}} - \phi_i^{\mathrm{p}}\right)^2\right\}}{N}}, \tag{6}$$

where ρ_a is the apparent resistivity in ohm-m, ϕ is the phase in degree, superscripts o and p stand for 'observed' and 'predicted', respectively, and w is a constant controlling the relative importance of the phase to the apparent resistivity (Sasaki 2004).

Phases (ϕ_{xy} and ϕ_{yx}) and logarithmic values of apparent resistivities [$\ln(\rho_{xy})$ and $\ln(\rho_{yx})$] are used as MT data in this study, where subscripts xy and yx denote Zxy and Zyx modes, respectively; thus, N is defined as

$$N = 4 \times N_{\mathrm{site}} \times N_{\mathrm{freq}} \tag{7}$$

where N_{site} and N_{freq} are the numbers of sites and frequencies, respectively. An optimum value of λ in solving eq. (4) is searched to minimize R at each iteration (Sasaki 2004).

3 FORWARD MODELLING

Predicted MT data are generated through forward modelling to evaluate $\Delta\mathbf{d}$ in eq. (4). From Maxwell's equations with $e^{i\omega t}$ time dependence, neglecting displacement currents, a second-order vector Helmholtz equation for electric fields $\mathbf{E}$ can be obtained as

$$\nabla\times\nabla\times\mathbf{E} + i\omega\mu_0\sigma\mathbf{E} = \mathbf{J}_{\mathrm{s}}, \tag{8}$$

where ω is the angular frequency, μ_0 is the magnetic permeability of the free space ($4\pi\times10^{-7}$ H m^{-1}), σ is the conductivity and $\mathbf{J}_{\mathrm{s}}$ is an impressed source. Decomposing the electric field into primary ($\mathbf{E}_{\mathrm{p}}$) and secondary ($\mathbf{E}_{\mathrm{s}}$) electric fields as

$$\mathbf{E} = \mathbf{E}_{\mathrm{p}} + \mathbf{E}_{\mathrm{s}} \tag{9}$$

yields

$$\nabla\times\nabla\times\mathbf{E}_{\mathrm{s}} + i\omega\mu_0\sigma\mathbf{E}_{\mathrm{s}} = -i\omega\mu_0(\sigma - \sigma_{\mathrm{p}})\mathbf{E}_{\mathrm{p}}, \tag{10}$$

with

$$\nabla\times\nabla\times\mathbf{E}_{\mathrm{p}} + i\omega\mu_0\sigma_{\mathrm{p}}\mathbf{E}_{\mathrm{p}} = \mathbf{J}_{\mathrm{s}}, \tag{11}$$

where σ_{p} indicates the conductivity of a background medium. Eq. (10) enables us to avoid a singularity problem at the source point (Unsworth *et al*. 1993).

For MT modelling, eq. (8) is solved for $\mathbf{J}_{\mathrm{s}} = 0$, using the algorithm developed by Sasaki (1999). The algorithm is based on a finite difference method with a staggered grid (Yee 1966) and solves the resulting system of equations using a bi-conjugate gradient (BICG) method, preconditioned with an incomplete Cholesky decomposition for diagonal sub-blocks of the coefficient matrix (Sasaki 1999). A static divergence correction is used to make the divergence of the resulting solution zero, accelerating the convergence rate, especially at low frequencies (Smith 1996). Given the solution of electric fields in eq. (8), magnetic fields are obtained from

$$\nabla\times\mathbf{E} = -i\omega\mu_0\mathbf{H}. \tag{12}$$

4 SENSITIVITIES

The sensitivity of an MT field with respect to the conductivity of an inversion block can be obtained efficiently from an adjoint-equation method, based on the reciprocity principle (McGillivray *et al*. 1994).

For example, the sensitivity of the x-component of electric fields, E_x, at a measurement site with respect to the conductivity of the mth block, σ_m, having a volume of V is given by

$$\frac{\partial E_x}{\partial \sigma_m} = \int_V \mathbf{E}^{Jx} \cdot \mathbf{E}\, \mathrm{d}V, \tag{13}$$

where $\mathbf{E}$ and $\mathbf{E}^{Jx}$ denote the electric fields due to a MT plane-wave source and an x-directed unit electric dipole source J_x, located at the measurement site, respectively. Note that $\mathbf{E}$ was previously calculated to evaluate $\Delta\mathbf{d}$, whereas $\mathbf{E}^{Jx}$ is computed using eqs (9)–(11), where the secondary electric fields $\mathbf{E}_{\mathrm{s}}^{Jx}$ are derived with forward modelling. The primary electric fields $\mathbf{E}_{\mathrm{p}}^{Jx}$ are computed analytically. Similarly, the other sensitivities of horizontal electric and magnetic fields, $\partial E_y/\partial\sigma_m$, $\partial H_x/\partial\sigma_m$ and $\partial H_y/\partial\sigma_m$, are calculated from the electric fields due to electric and magnetic dipole sources, J_y, M_x and M_y.

In 3-D, eq. (10) must be solved for four dipole sources at every MT measurement site and frequency to construct the exact sensitivity matrix ($\boldsymbol{E}$). Thus, construction of $\boldsymbol{E}$ requires a large number of forward calculations, even though the efficient adjoint-equation method is employed. Most of the computation time for constructing $\boldsymbol{E}$ is spent on computing electric fields due to dipole sources, $\mathbf{E}^{Ji}$ ($J_i = J_x$, J_y, M_x or M_y), specifically on computing $\mathbf{E}_{\mathrm{s}}^{Ji}$ in eq. (10). To avoid the computational burden, $\mathbf{E}_{\mathrm{s},k}^{Ji}$ at the kth iteration is replaced with $\mathbf{E}_{\mathrm{s},k-1}^{Ji}$, used in the previous iteration as

$$\mathbf{E}_k^{Ji} = \mathbf{E}_{\mathrm{p},k}^{Ji} + \mathbf{E}_{\mathrm{s},k}^{Ji} \approx \mathbf{E}_{\mathrm{p},k}^{Ji} + \mathbf{E}_{\mathrm{s},k-1}^{Ji}. \tag{14}$$

This approximation is reasonable when the current model is close to a base model or the model in the previous iteration (the third term on the right-hand side in eq. 3). $\mathbf{E}_{\mathrm{p}}^{Ji}$ is calculated analytically for a homogeneous half-space having the resistivity of the block on which a receiver under consideration exists. To efficiently evaluate $\mathbf{E}_{\mathrm{p}}^{Ji}$, a linear filter developed by Guptasarma & Singh (1997) was utilized. The resulting approximate sensitivity is designated as $\boldsymbol{A}$.

The inversion algorithm used in this study always begins with a homogeneous half-space model in which the electric fields due to a dipole source or a plane-wave source can be calculated analytically. The exact sensitivities for the initial model can be obtained analytically and are called $\boldsymbol{I}$ to distinguish them from $\boldsymbol{E}$ at the kth iteration ($k \neq 1$). To compare $\boldsymbol{A}$ with other approximate sensitivities, updated sensitivities ($\boldsymbol{U}$) derived from the Broyden's method (Loke & Barker 1996) are utilized. $\boldsymbol{U}$ has been successfully employed for an efficient 3-D MT inversion by Sasaki (2004).

Thus, four kinds of sensitivities, $\boldsymbol{I}$, $\boldsymbol{E}$, $\boldsymbol{U}$ and $\boldsymbol{A}$, are utilized in the inversion. Note that the secondary electric fields during inversion iterations are updated only when $\boldsymbol{E}$ is employed. To examine the efficiency and accuracy of $\boldsymbol{A}$, results obtained from inversion procedures with $\boldsymbol{A}$ but without $\boldsymbol{U}$ are compared with those with $\boldsymbol{U}$ but without $\boldsymbol{A}$. For notational simplicity, inversion procedures are named after the order of sensitivities employed during inversion; for example, if inversion is conducted by using sensitivities in such an order of $\boldsymbol{I}$, $\boldsymbol{A}$, $\boldsymbol{E}$ and $\boldsymbol{U}$, it is called as *IAEU*.

5 PARALLEL COMPUTATION

To reduce the large computation time of the 3-D inversion algorithm to a practical level, the calculation of a full sensitivity matrix can be parallelized. An inversion based on the GN-approach is composed of three main parts: (1) constructing a sensitivity matrix; (2) solving the observation equation (eq. 4) and (3) MT modelling to compute the data misfit. Almost all computation time is spent on constructing $\boldsymbol{E}$. Since the sensitivities of the MT responses at one frequency are independent of those at another frequency, the construction of a full sensitivity matrix can be parallelized using the same number of processors as that of frequencies; each processor computes only the sensitivities at a specific frequency. The host processor solves the observation equation after gathering sensitivities from each processor and constructing the full sensitivity matrix. MT modelling can also be parallelized in the same way. Although the parallelization is very basic, it is quite effective to reduce the huge computational burden of a 3-D inversion based on the GN-approach.

When computing sensitivities $\boldsymbol{A}$, the reduction of computation time by the parallelization is minimal because $\boldsymbol{A}$ does not require time-consuming calculation of secondary electric fields. The parallelization, however, has an alternate merit of reducing memory requirements because one processor needs to store only the secondary electric fields at a specific frequency. All computations in this study were performed on a HAMEL cluster system with 256 nodes of IBM x335 server. Each node has two processors of Intel Pentium IV Xeon DP 2.8 GHz (KISTI 2005).

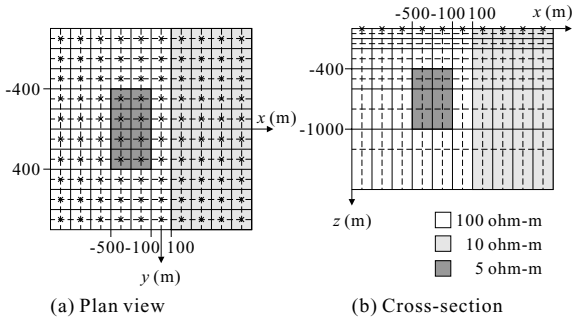

Figure 1. Plan (a) and cross-sectional (b) views of a test model, which consists of a 5 ohm-m conductor and a vertical contact between half-spaces with resistivities of 100 and 10 ohm-m. The conductor has dimensions of 400 × 800 × 600 m and is embedded at a depth of 400 m. Crosses indicate MT stations. Solid lines represent inversion blocks, whereas both solid and dotted lines indicate the mesh used for forward modelling.

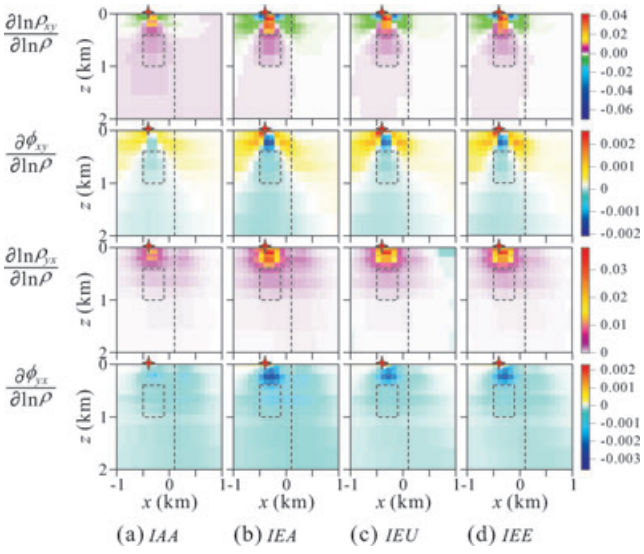

Figure 2. Cross-sections of sensitivities of MT responses at the third iteration for the inversion procedures, *IAA* (a), *IEA* (b), *IEU* (c) and *IEE* (d), for the model shown in Fig. 1. Red crosses represent receivers at (–400 m, –100 m, 0 m) and dotted lines the conductor and the vertical contact. Each row shows $\partial\ln(\rho_{xy})/\partial\ln(\rho)$, $\partial\phi_{xy}/\partial\ln(\rho)$, $\partial\ln(\rho_{yx})/\partial\ln(\rho)$ and $\partial\phi_{yx}/\partial\ln(\rho)$.

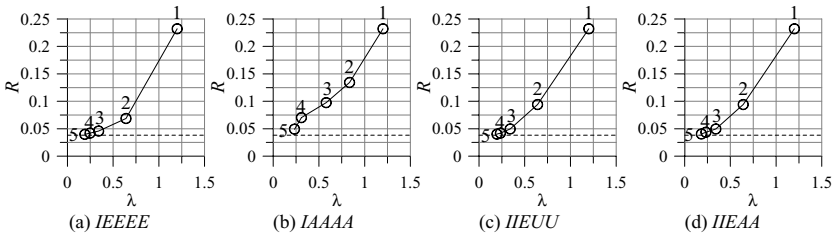

Figure 3. Lagrange multipliers and rms data misfits during inversion of synthetic MT data, generated from the model shown in Fig. 1; *IEEEE* (a), *IAAAA* (b), *IIEUU* (c) and *IIEAA* (d). Dotted lines show a noise level of 3.8 per cent, which is added to the synthetic data, and the numeral values represent the iteration numbers of the procedures.

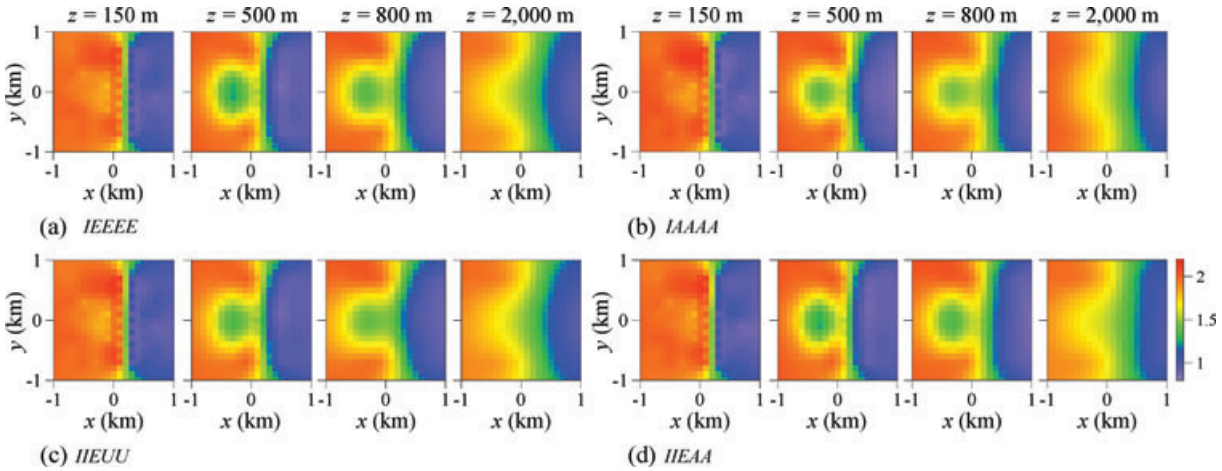

Figure 4. Horizontal depth slices of models obtained from the inversion of synthetic MT data for the model shown in Fig. 1. The slices are at depths of 150, 500, 800 and 2000 m.

6 INVERSION EXPERIMENTS

The approximate sensitivity $\boldsymbol{A}$ was tested through an inversion study using a synthetic MT data set and two field MT data sets. The sensitivity analysis was applied to synthetic MT data to verify the accuracy of the approximate sensitivities, $\boldsymbol{A}$. Using field data obtained in Pohang, Korea, the variable weighting to static shifts in eq. (3) is validated against the constant weighting in eq. (2). The efficiency of $\boldsymbol{A}$ and parallelization is verified by comparing computation time in 3-D inversion of field data. The number of processors used for parallel computation is equal to the number of frequencies.

6.1 Synthetic data

The test model consists of a 5 ohm-m conductor and a vertical contact between two quarter-spaces with resistivities of 100 and 10 ohm-m (Fig. 1; Sasaki 2004). Synthetic MT data were generated at 100 stations for seven frequencies, ranging from 0.1 to 100 Hz. Gaussian random noise with a standard deviation of 1.5 per cent was added to the synthetic impedance data prior to inversion. This is equal to standard deviations of 3 per cent and 0.9° for the apparent resistivity and phase, respectively. Static shifts were applied to the apparent resistivities. The static shift coefficients were random values selected from a Gaussian distribution with a mean of zero and a standard deviation of 0.5. A homogeneous half-space of 30 ohm-m was used as an initial model and parameters α, β and w are set to 0.2, 1.0 and 0.05, respectively.

To validate approximate sensitivities, sensitivities are calculated at 0.1 Hz for apparent resistivities and phases in both Z*xy*

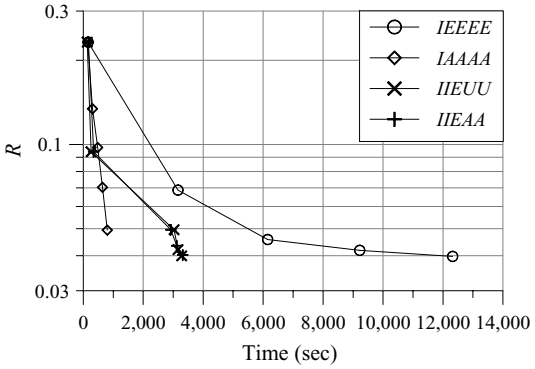

Figure 5. The rms data misfits versus computation times as a function of iteration number for the four inversion procedures, *IEEEE*, *IAAAA*, *IIEAA* and *IIEUU*.

and Z*yx* modes: $\partial \ln(\rho_{xy})/\partial \ln(\rho)$, $\partial \ln(\rho_{yx})/\partial \ln(\rho)$, $\partial \phi_{xy}/\partial \ln(\rho)$ and $\partial \phi_{yx}/\partial \ln(\rho)$. The receiver is located at (−400 m, −100 m, 0 m) in the resistive side of the vertical contact. We compare sensitivities at the third iteration, that is, *IAA*, *IEU*, *IEA* and *IEE* (Fig. 2). $\boldsymbol{A}$ at the third iteration of *IAA* is generally smaller than $\boldsymbol{E}$ of *IEE*, however, the overall trend is very similar to $\boldsymbol{E}$. $\boldsymbol{U}$ of *IEU* and $\boldsymbol{A}$ of *IEA* produce almost the same values as $\boldsymbol{E}$. In particular, since $\boldsymbol{A}$ is more similar to $\boldsymbol{E}$ than $\boldsymbol{U}$ in the conductive side of the vertical contact, $\boldsymbol{A}$ can resolve the conductor well from the vertical contact and be a good substitute for $\boldsymbol{E}$ after $\boldsymbol{E}$ is applied.

Next, we compare results from the four inversion procedures: *IEEEE*; *IAAAA*; *IIEUU* and *IIEAA*. We choose *IEEEE* as a reference

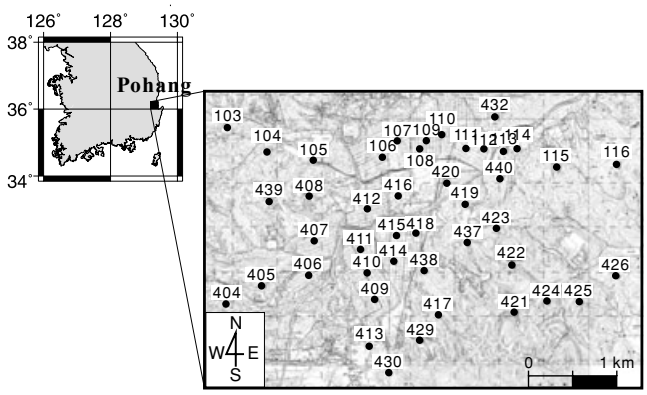

Figure 6. A map showing 44 MT sites in the Pohang area, Korea.

procedure since it is supposed to give the most accurate inversion results. *IIEAA* and *IAAAA* are selected as the procedures employing ***A***, whereas *IIEUU* was selected for comparison with *IIEAA* and *IAAAA*. All these procedures effectively reduce both R and λ (Fig. 3) and resolve the vertical contact and the conductor as shown in the horizontal slices of the inversion model (Fig. 4). Though final R of *IAAAA* is slightly larger than the other procedures with ***E***, *IAAAA* gives clear subsurface images in very short computation time, only 6 per cent of that of *IEEEE* (Fig. 5). The methods including ***A***, *IAAAA* and *IIEAA*, can separate the conductor from the vertical contact, whereas *IIEUU* yields a smeared image at a depth of 800 m.

6.2 Field data from Pohang, Korea

In Pohang, Korea, MT surveys were conducted for low-enthalpy geothermal exploration in 2002 and 2003 by the Korea Institute of Geoscience and Mineral Resources (Lee *et al*. 2007). We perform 3-D inversion of MT data from 44 stations (Fig. 6) at 13 frequencies, ranging from 0.0159 to 66 Hz. The noise floor was assumed to be 1.5 per cent for the MT impedance. Parameters α and β are set to 0.2 and 1.0, respectively. In the inversion, a 66 × 55 × 33 grid is used for forward modelling, and the subsurface is divided into 1950 (15 × 10 × 13) blocks of unknown resistivity. An initial model is a homogeneous half-space with the log-average resistivity of observed apparent resistivities, 14.65 ohm-m.

6.2.1 Analysis of the static shift weighting factor

To validate the variable weighting to static shifts, $\lambda\beta$, in eq. (3), inversion results from the two objective functions with fixed and variable weightings, eqs (2) and (3), are compared. Inversion results are derived from using three initial models: homogeneous half-spaces of (1) 14.65 ohm-m, the log-average resistivity of observed apparent resistivities; (2) 30 ohm-m and (3) 50 ohm-m. β is set to 8.0 for the fixed weighting and 1.0 for the variable weighting in inversion procedure *IUUEUUUUU*.

As static shifts are only affected by the geological features near the measurement sites (deGroot-Hedlin 1991), similar static shifts should be recovered regardless of the initial model used, if the inversion is fully converged. However, when the fixed weighting was used, the recovered static shifts were observed to

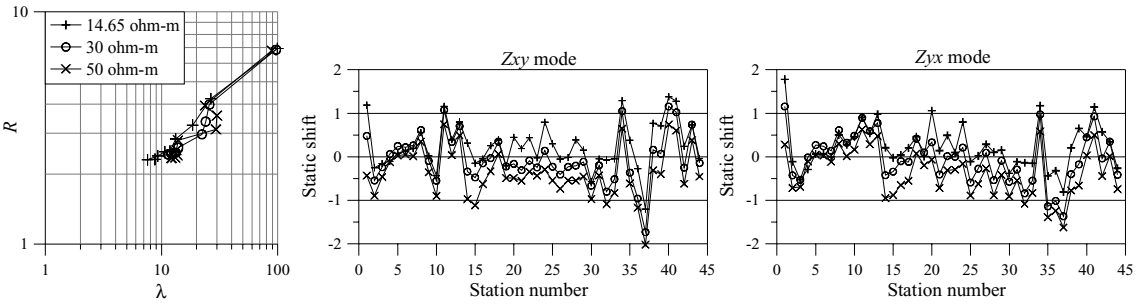

(a) *rms* data misfit (b) static shift

Figure 7. The rms data misfits (a) and static shifts in the Z*xy* and Z*yx* modes (b), for the three initial models using the objective function with a fixed weighting (eq. 2). The resistivities of three initial models are 14.65, the log-average value of observed apparent resistivities (pluses), 30 (circles) and 50 ohm-m (crosses), respectively.

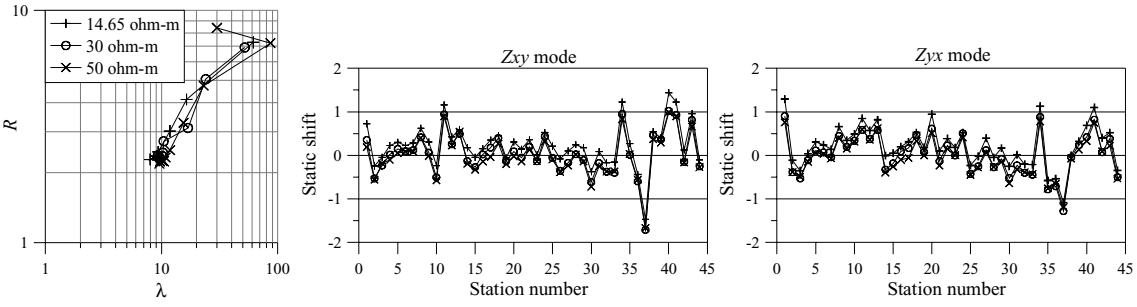

(a) *rms* data misfit (b) static shift

Figure 8. The rms data misfits (a) and static shifts in the Z*xy* and Z*yx* modes (b), for the three initial models using the objective function with a variable weighting (eq. 3). The resistivities of three initial models are 14.65, an average value of observed apparent resistivities (pluses), 30 (circles) and 50 ohm-m (crosses), respectively.

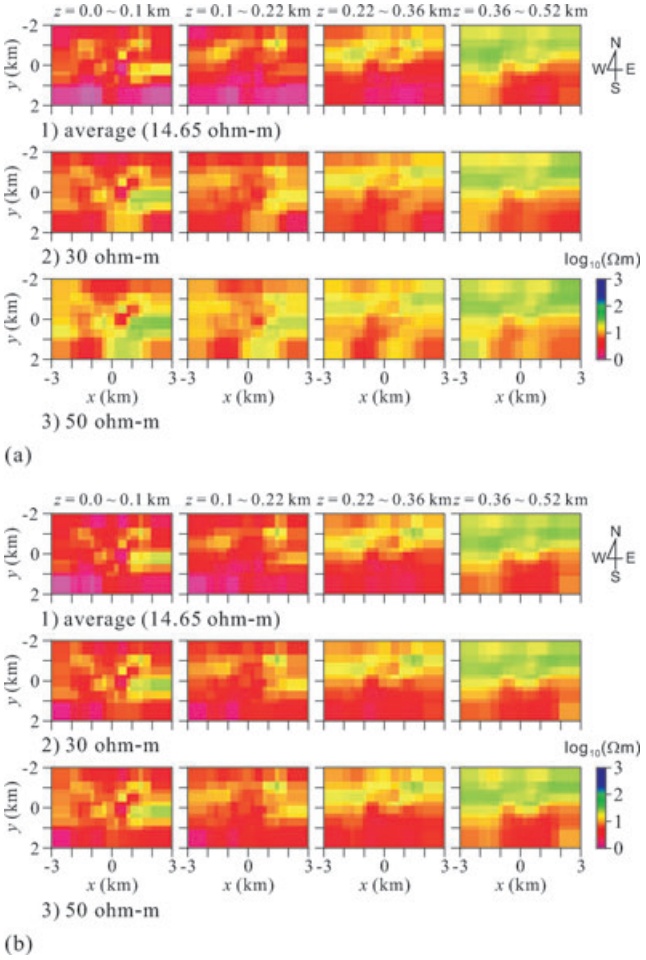

Figure 9. Inversion models at the depths from surface to 0.52 km, for the three initial models using the objective functions with fixed (a) and variable (b) weightings. The resistivities of three initial models are 14.65, the log-average value of observed apparent resistivities (first row), 30 (second row), and 50 ohm-m (third row).

depend on the initial resistivity model (Fig. 7b). At the same time, the resistivity values recovered by the inversion varied in the top 0.52 km of the model (Fig. 9a). The inversions for all the three initial models are stopped after nine iterations, when no more significant decrease of data misfit was made, as shown in Fig. 7a. Since λ varies widely from about 70 at the first iteration to 5 at the final iteration (Fig. 7a), β is relatively small at earlier iterations to cause large static shifts, whereas relatively large β yields small static shifts at later iterations. As a result, static shifts are sensitive to the resistivity of an initial model and can give rise to a significant effect in the inversion model.

Inversion with variable weighting $\lambda\beta$, however, yields almost the same recovered static shifts and inversion model at shallow depths for all the three initial models (Figs 8b and 9b), reducing R to lower values (Fig. 8a). Because $\lambda\beta$ controls the relative importance of static shifts to both model roughness and data misfit, inversion results are not affected by the resistivity of an initial model. Thus, the scheme using $\lambda\beta$ is effective to obtain more reasonable results when λ varies widely during inversion.

6.2.2 *Analysis on **A***

To validate the efficiency and accuracy of ***A*** on field data, six inversion procedures were tested: *IEEEEEEEE*; *IAAAAAAAA*; *IAEAEAEAE*; *IUEUEUEUE*; *IAAEAAAAA* and *IUUEUUUUU* (from now on, we call them simply *IEEE*, *IAAA*, *IAEA*, *IUEU*, *IAAE* and *IUUE*, respectively). *IEEE* was selected as a reference procedure, whereas *IAAA* was chosen as a procedure that never used ***E***. We choose *IAEA* to examine the inversion results obtained when ***A*** and ***E*** were used alternately. *IAAE* was selected as the most efficient procedure after we have tested many combinations of sensitivities. *IUEU* and *IUUE* are selected for comparison with *IAEA* and *IAAE*, respectively. After nine iterations, all the six procedures reduced both R and λ effectively (Fig. 10).

Six depth slices of the inversion model are shown in Fig. 11. Models from *IEEE* (Fig. 11a) show typical features of the Pohang area since *IEEE* uses exact sensitivities, although enormous computation time was required (Fig. 12). A thick surface layer with resistivities less than 10 ohm-m extends to a depth of about 300 m in the northern part and about 500 m in the southern part. The interface between the conductive and resistive regions dips in the NNE–SSW direction. Below the conductive surface layer, the resistivity increases gradually with depth, and a resistive layer of more than 100 ohm-m exists at depths from 900 m to 2 km in the northern part. The resistivity decreases again below 2 km, and a zone of very low resistivity is observed in the deep southwestern and northeastern parts of the model.

IAAA yields different models to those obtained from *IEEE*, at greater depths (Fig. 11b). As a result, in the case of field MT data, ***E*** should be used at least once to reliably recover the subsurface resistivity structure. In contrast, *IAEA* gives almost the same inversion model as those obtained from *IEEE* over the entire depth range (Fig. 11c). *IUEU* generates similar resistivity models to those obtained from *IEEE* but with slightly lower resistivities at depths of ∼1–2 km (Fig. 11d). Although *IAEA* and *IUEU* recover the subsurface resistivity structure successfully, the computation times are still long, about 40 per cent of that of *IEEE* (Fig. 12).

For more efficient 3-D inversion, two methods are tested, *IAAE* and *IUUE*. The final rms data misfits are 2.13 and 2.30, respectively, and the computation times are lowered to about 16 per cent of that of *IEEE*. Furthermore, the inversion models from *IAAE* are very similar to those from *IEEE* over the whole depth range (Fig. 11e).

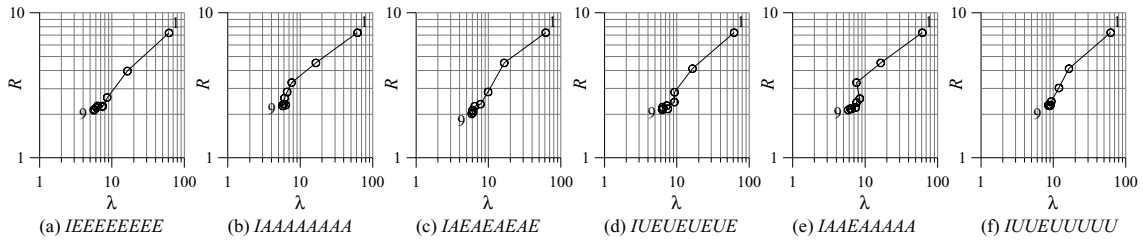

Figure 10. Lagrange multipliers and rms data misfits for the six procedures of field data obtained in Pohang, Korea. Only the first and last iteration numbers are shown on the graphs.

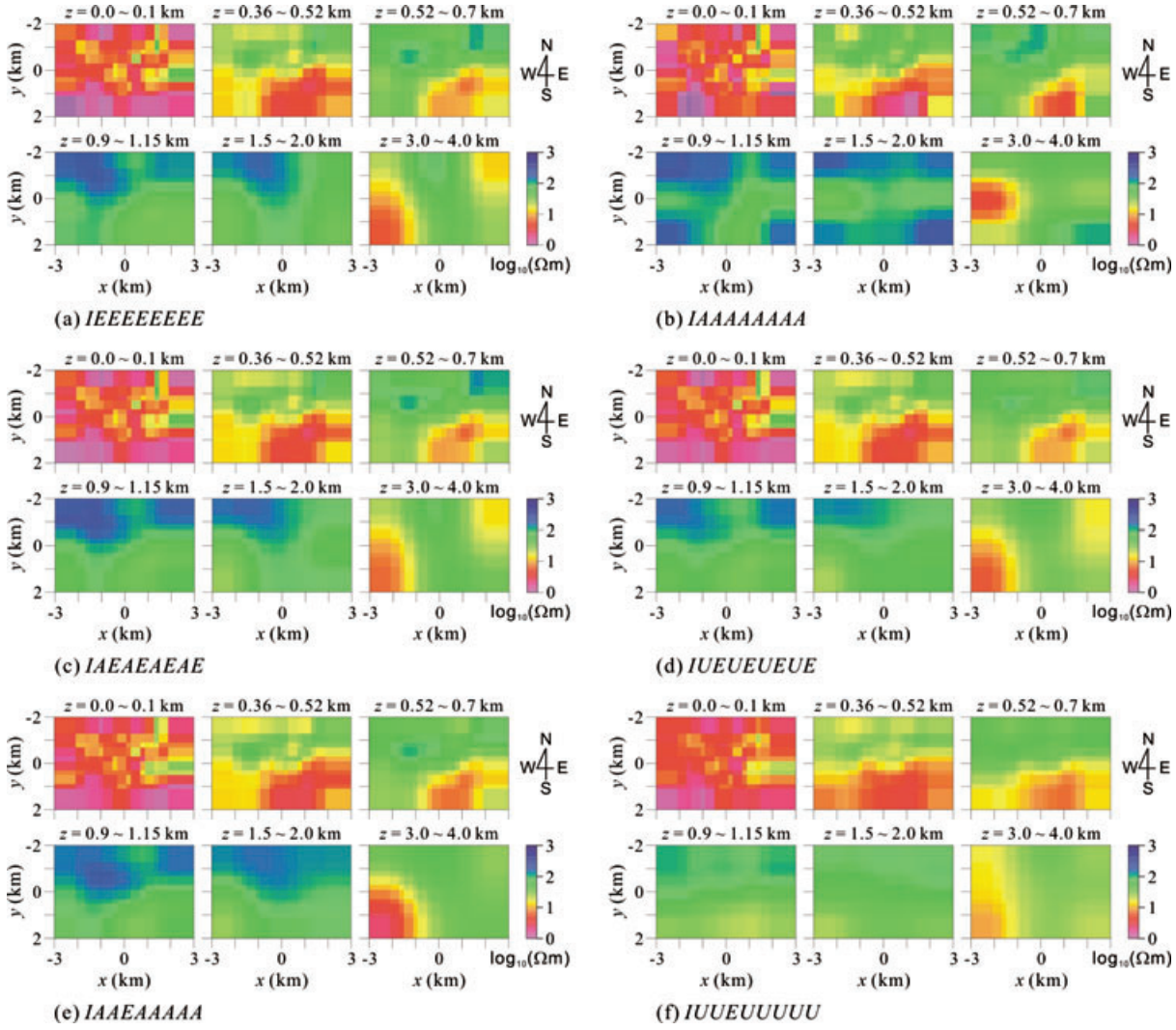

Figure 11. Horizontal depth slices of models obtained from inversion of field data obtained in Pohang, Korea. Six procedures of *IEEEEEEEEE* (a), *IAAAAAAAAA* (b), *IAEAEAEAEA* (c), *IUEUEUEUEU* (d), *IAAEAAAAAA* (e) and *IUUEUUUUUU* (f) are compared.

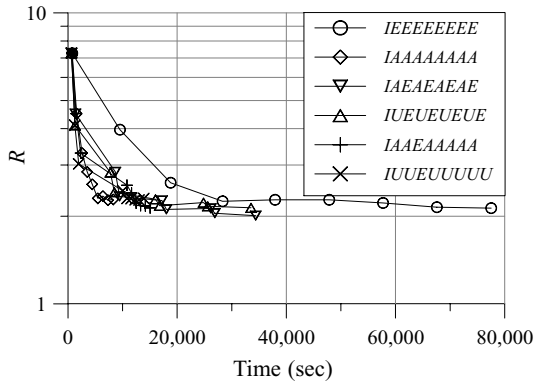

Figure 12. The rms data misfits versus computation times as a function of inversion iteration for the six inversion procedures, *IEEEEEEEE*, *IAAAAAAAA*, *IAEAEAEAE*, *IUEUEUEUE*, *IAAEAAAAA* and *IUUEUUUUU*.

However, *IUUE* produces a model that was too smooth below a depth of 500 m (Fig. 11f). Consequently, *IAAE* is considered to be the most effective procedure for 3-D inversion of the field MT data obtained in Pohang, Korea.

Table 1. Computation times based on the serial and parallel computation.

	Serial (s)	Parallel (s)
Constructing ***E***	58 126	5532
Solving observation equation	55	86
MT modelling	369	109
One iteration step	60 294	6335

6.2.3 Analysis for parallel computation

Although the computation time of *IEEE* is the longest among the six inversion procedures, it takes only about 1 day if parallel computation is used (Fig. 12). In serial computation, the computation time for computing ***E*** is 58 126 s, which is about 96 per cent of the total computation time for one iteration, 60 294 s (Table 1). The parallelization reduces the computation time to 5 532 s, less than 1/10 of the serial computation time (Table 1). The reduced computation time is slightly longer than $1/N_{\text{freq}}$. This is mainly because all processors must finish their calculations to allow the host processor to construct the full sensitivity matrix, and modelling at lower frequencies needs more computation time (Smith 1996).

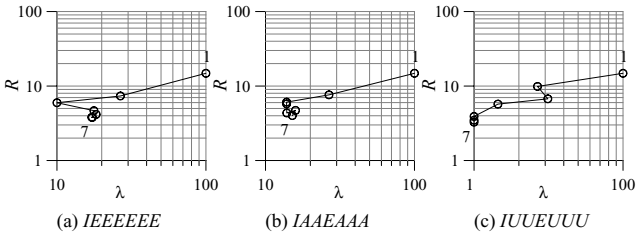

Figure 13. Lagrange multipliers and rms data misfits for the three procedures of field data in Flores Island, Indonesia. Only the first and last iteration numbers are shown on the graphs.

6.3 Field data in Bajawa, Indonesia

The approximate sensitivity $\boldsymbol{A}$ was applied to inversion of field MT data obtained in the Bajawa geothermal field in central Flores Island, eastern Indonesia (Uchida *et al*. 2002). Three inversion procedures of *IEEEEEE*, *IUUEUUU* and *IAAEAAA* were employed as in the inversion of the Pohang data set. MT data collected at 36 sites were inverted with 12 frequencies ranging from 0.0352 to 60 Hz. The noise floor was assumed to be 1.5 per cent for the MT impedance and parameters α and β are set to 0.2 and 1.0, respectively. The initial model is a homogeneous half-space of 6.68 ohm-m, the log-average value of observed apparent resistivities.

After seven iterations, the three inversion procedures had converged, although the final rms data misfits were still relatively high (3–4; Fig. 13). The resistivity structure at Bajawa is known to consist of three main layers (Uchida *et al*. 2002): a thin, resistive surface layer; a low resistivity layer of 450 m thick and a resistive basement. Inversion models obtained from *IEEEEEE* clearly show a three-layered structure (Fig. 14a). *IAAEAAA* produces a similar inversion model to that obtained from *IEEEEEE* (Fig. 14b). *IUUEUUU*, however, yields slightly different models, below a depth of 2 km, from *IEEEEEE* (Fig. 14c), although the final rms data misfit is reduced to a lower level of 3.27. The computation times of *IAAEAAA* and *IUUEUUU* are less than 30 per cent of that of *IEEEEEE* (Fig. 15). For Bajawa data, *IAAEAAA* produces more similar results to those from *IEEEEEE* than *IUUEUUU*.

7 CONCLUSIONS

For the efficient 3-D inversion of static-shifted MT data, approximate sensitivities can be used. They are computed more efficiently by replacing secondary electric fields with those calculated in the previous iteration. The inversion is further speeded up by using parallel computation for the calculation of sensitivities. These changes reduce both the computation time and memory requirements to a practical level. The effectiveness of using approximate sensitivities was validated through inversion of both synthetic and field MT data obtained in Korea and Indonesia. Sensitivity analysis using synthetic data demonstrates that the approximate sensitivity is an effective substitute for the exact sensitivity. A variable weighting of the static shifts is employed to yield more reliable resistivity images from static-shifted MT data. The field-data examples demonstrate that the variable weighting to static shifts is effective in recovering both 3-D resistivity structures and static shifts.

ACKNOWLEDGMENTS

MT surveys in Pohang were carried out under the support of Basic Research Project of Korea Institute of Geoscience and Mineral Resources (KIGAM). This work was supported by Korea Research Foundation Grant, funded by the Korea Government (MOEHRD; KRF-2006-311-D00985) and Brain Korea 21 Project of the Ministry of Education. All computations are conducted on the 'Hamel cluster system' of supercomputing centre in Korea Institute of Science and Technology Information (KISTI). We are grateful to Yutaka Sasaki for allowing us to use and modify his 3-D MT inversion code and to

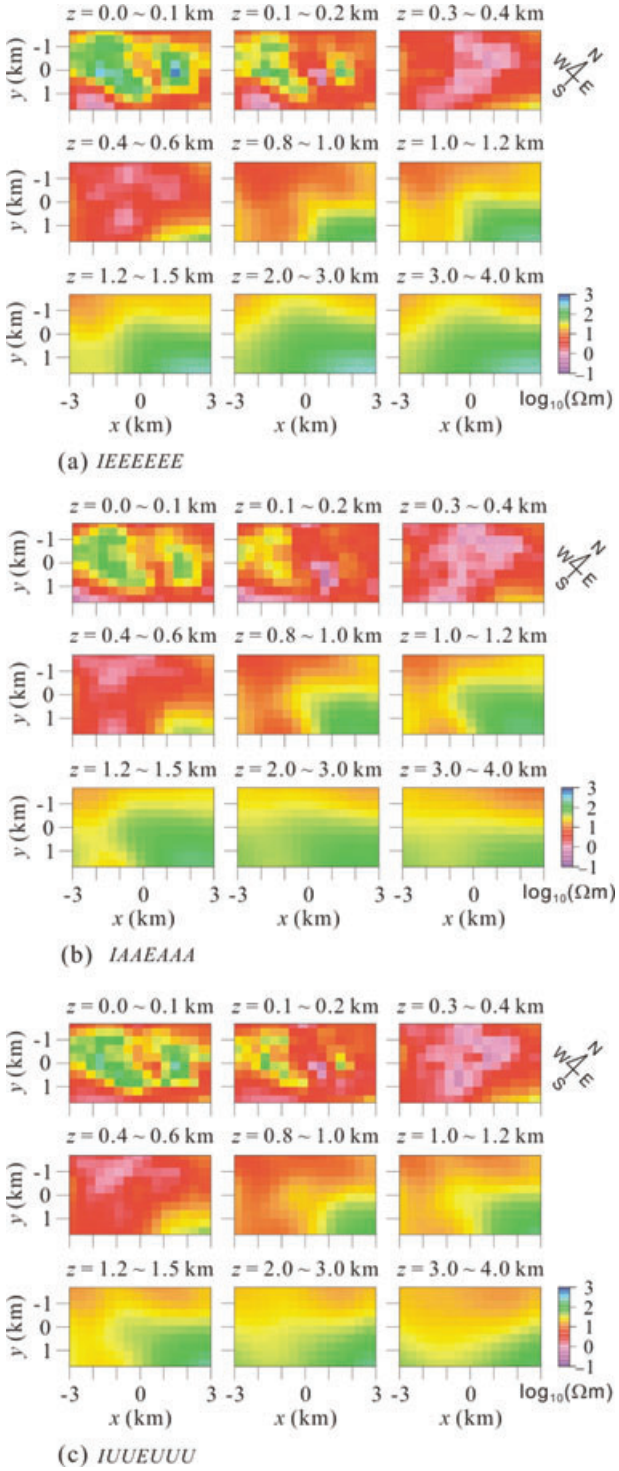

Figure 14. Horizontal depth slices of models obtained from inversion of field MT data from Flores Island, Indonesia. Three procedures of *IEEEEEE* (a), *IAAEAAA* (b) and *IUUEUUU* (c) are compared.

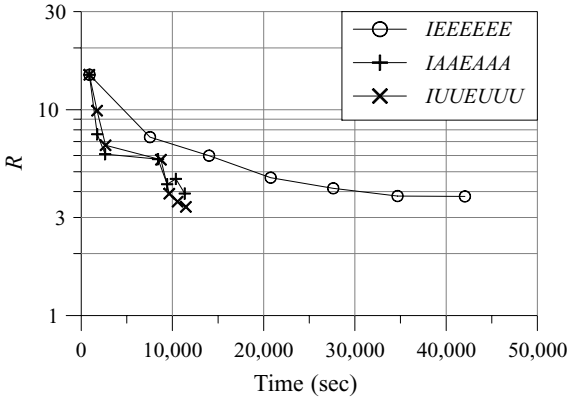

Figure 15. The rms data misfits versus computation times as a function of inversion iteration for the three inversion procedures, *IEEEEEE*, *IAAEAAA* and *IUUEUUU*.

Toshihiro Uchida for permitting us to use the field data in Bajawa. Comments by Martyn Unsworth, Randy Mackie and an anonymous reviewer improved this paper.

REFERENCES

deGroot-Hedlin, C., 1991. Removal of static shift in two dimensions by regularized inversion, *Geophysics,* **56,** 2102–2106.

Farquharson, C.G. & Oldenburg, D.W., 1999. Approximate sensitivities for multidimensional electromagnetic inversion, in *Three-dimensional Electromagnetics,* eds Oristaglio, M.L. & Spies, B.R., Soc. Expl. Geophys., pp. 256–264.

Garcia, X., Ledo, J. & Queralt, P., 1999. 2D inversion of 3D magnetotelluric data: the Kayabe dataset, *Earth Planets Space,* **51,** 1135–1143.

Guptasarma, D. & Singh, B., 1997. New digital linear filters for Hankel J_0 and J_1 transforms, *Geophys. Prospect.*, **45,** 745–762.

Korea Institute of Science and Technology Information (KISTI), 2005. User manual of KISTI cluster system (HAMEL) (in Korean).

Lee, T.J., Uchida, T., Sasaki, Y. & Song, Y., 2003. Characteristics of static shift in 3-D MT inversion, *Mulli-Tamsa,* **6,** 199–206.

Lee, T.J., Song, Y. & Uchida, T., 2007. Three-dimensional magnetotelluric surveys for geothermal development in Pohang, Korea, *Explor. Geophys.,* **38,** 44–49.

Loke, M.H. & Barker, R.D., 1996. Practical technique for 3D resistivity surveys and data inversion, *Geophys. Prospect.*, **44,** 499–523.

Mackie, R.L. & Madden, T.R., 1993. Three-dimensional magnetotelluric inversion using conjugate gradients, *Geophys. J. Int.,* **115,** 215–229.

McGillivray, P.R., Oldenburg, D.W., Ellis, R.G. & Habashy, T.M., 1994. Calculation of sensitivities for the frequency-domain electromagnetic problem, *Geophys. J. Int.,* **116,** 1–4.

Newman, G.A. & Alumbaugh, D.L., 2000. Three-dimensional magnetotelluric inversion using non-linear conjugate gradients, *Goephys., J. Int.,* **140,** 410–424.

Ogawa, Y. & Uchida, T., 1996. A two-dimensional magnetotelluric inversion assuming Gaussian static shift, *Geophys. J. Int.*, **126,** 69–76.

Rodi, W. & Mackie, R.L., 2001. Nonlinear conjugate gradients algorithm for 2-D magnetotelluric inversion, *Geophysics,* **66,** 174–187.

Sasaki, Y., 1999. Three-dimensional frequency-domain electromagnetic modeling using the finite-difference method (Japanese with English abstract), *Butsuri-Tansa,* **52,** 421–431.

Sasaki, Y., 2004. Three-dimensional inversion of static-shifted magnetotelluric data, *Earth Planets Space,* **56,** 239–248.

Siripunvaraporn, W., Egbert, G., Lenbury, Y. & Uyeshima, M., 2005. Three-dimensional magnetotelluric inversion: data-space method, *Phys. Earth planet. Inter.,* **150,** 3–14.

Smith, J.T., 1996. Conservative modeling of 3-D electromagnetic fields, Part II: biconjugate gradient solution and an accelerator, *Geophysics,* **61,** 1319–1324.

Smith, J.T. & Booker, J.R., 1991. Rapid inversion of two- and three-dimensional magnetotelluric data, *J. geophys. Res.*, **96,** 3905–3922.

Takasugi, S., Tanaka, N., Kawakami, N. & Muramatsu, S., 1992. High spatial resolution of the resistivity structure revealed by a dense network MT measurement – a case study in the Minamikayabe area, Hokkaido, Japan, *J. Geomag. Geoelectr.,* **44,** 289–308.

Tournerie, B. & Chouteau, M., 2005. Three-dimensional magnetotelluric survey to image structure and stratigraphy of a sedimentary basin in Hungary, *Phys. Earth planet. Inter.,* **150,** 197–212.

Uchida, T., Lee, T.J., Honda, M. & Andan, A., 2002. 2-D and 3-D interpretation of magnetotelluric data in the Bajawa geothermal field, central Flores, Indonesia, *Bull. Geol. Surv. Japan,* **53,** 265–283.

Unsworth, M.J., Travis, B.J. & Chave, A.D., 1993. Electromagnetic induction by a finite electric dipole source over a 2-D earth, *Geophysics,* **58,** 198–214.

Yee, K.S., 1966. Numerical solution of initial boundary value problems involving Maxwell's equation in isotropic media, *IEEE, Trans. Antenn. Prop.*, **AP-14,** 302–307.

Zhdanov, M.S., Fang, S. & Hursan, G., 2000. Electromagnetic inversion using quasi-linear approximation, *Geophysics,* **65,** 1501–1513.